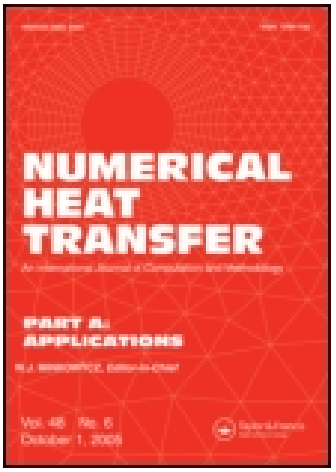

Numerical Heat Transfer, Part A: Applications: An International Journal of Computation and Methodology
Publication details, including instructions for authors and subscription information:
http://www.tandfonline.com/loi/unht20

Estimation of a Location- and Time-Dependent High-Magnitude Heat Flux in a Heat Conduction Problem Using the Kalman Filter and the Approximation Error Model

César C. Pacheco[a], Helcio R. B. Orlande[a], Marcelo J. Colaço[a] & George S. Dulikravich[b]

[a] Department of Mechanical Engineering, Politecnica/COPPE, Federal University of Rio de Janeiro - UFRJ, Rio de Janeiro, RJ, Brazil

[b] Department of Mechanical and Materials Engineering, Florida International University - MAIDROC Laboratory, Miami, USA

Published online: 23 Jun 2015.

To cite this article: César C. Pacheco, Helcio R. B. Orlande, Marcelo J. Colaço & George S. Dulikravich (2015) Estimation of a Location- and Time-Dependent High-Magnitude Heat Flux in a Heat Conduction Problem Using the Kalman Filter and the Approximation Error Model, Numerical Heat Transfer, Part A: Applications: An International Journal of Computation and Methodology, 68:11, 1198-1219, DOI: 10.1080/10407782.2015.1037136

To link to this article: http://dx.doi.org/10.1080/10407782.2015.1037136

Numerical Heat Transfer, Part A, 68: 1198–1219, 2015

ISSN: 1040-7782 print/1521-0634 online
DOI: 10.1080/10407782.2015.1037136

ESTIMATION OF A LOCATION- AND TIME-DEPENDENT HIGH-MAGNITUDE HEAT FLUX IN A HEAT CONDUCTION PROBLEM USING THE KALMAN FILTER AND THE APPROXIMATION ERROR MODEL

César C. Pacheco[1], Helcio R. B. Orlande[1], Marcelo J. Colaço[1], and George S. Dulikravich[2]

[1]*Department of Mechanical Engineering, Politecnica/COPPE, Federal University of Rio de Janeiro – UFRJ, Rio de Janeiro, RJ, Brazil*

[2]*Department of Mechanical and Materials Engineering, Florida International University - MAIDROC Laboratory, Miami, USA*

This paper aims to estimate a location- and time-dependent high-magnitude heat flux in a heat conduction problem. The heat flux is applied on a small region of a surface of a flat plate, while transient temperature measurements are taken on the opposite surface. This inverse problem is solved using the Kalman filter and a reduced forward model, obtained by simplifications of a three-dimensional and nonlinear heat conduction problem. To deal with the modeling errors of this reduced model, the Approximation Error Model is used. The results show that excellent estimates can be obtained at feasible computational times.

INTRODUCTION

In recent years, modern and reliable available techniques for measuring temperature and heat flux have been developed. However, such measurements can still be very challenging, especially when involving fast transients and/or when the heat flux is imposed on small spots, thus resulting in large temperature gradients [1]. Other situations presenting a considerable level of difficulty involve complex geometries or hazardous environments, which might make direct measurements of heat flux impractical [2]. In such situations, surface heat fluxes need to be indirectly measured through the solution of an inverse problem, by using transient temperature measurements taken at other regions of the body.

In this article, a location- and time-dependent high-magnitude heat flux, applied on a surface of a flat plate, is estimated using transient temperature measurements taken on the opposite surface of the plate. The imposed heat flux could be originated by a moving high-power energy beam or modern electronic chips. Similar papers that addressed this problem using different techniques can be found in the literature, such as the Markov Chain Monte Carlo Method [1], the LSQR method

Received 27 December 2014; accepted 7 March 2015.

Address correspondence to Helcio R. B. Orlande, Department of Mechanical Engineering - Politecnica/COPPE, Federal University of Rio de Janeiro – UFRJ, Cid. Universitária, Rio de Janeiro, RJ 21941-972. E-mail: helcio@mecanica.coppe.ufrj.br

NOMENCLATURE

a	length of the plate, m
b	width of the plate, m
c	thickness of the plate, m
C	volumetric heat capacity of the complete model, J/m^3K
C^*	volumetric heat capacity of the reduced model, J/m^3K
$\mathbf{F}$	state vector evolution matrix
$\mathbf{H}$	observation matrix
I	number of volumes on the grid in the x direction
J	number of volumes on the grid in the y direction
k_T	thermal conductivity of the complete model, W/mK
k_T^*	thermal conductivity of the reduced model, W/mK
$\mathbf{K}$	Kalman gain matrix
M	number of approximation error samples
$\mathbf{P}_n$	posterior estimate of the error covariance matrix
$\mathbf{P}_{n\|n-1}$	prior estimate of the error covariance matrix
q	heat flux, W/m^2
q_0	heat flux constant value for the piecewise function, W/m^2
$\mathbf{q}$	vector of heat flux, W/m^2
$\mathbf{Q}$	covariance matrix of the evolution model noise
$\mathbf{R}$	covariance matrix of the observation model noise
T_c	temperature of the complete model, K
$\overline{T}$	mean temperature in the z direction, K
$\overline{\mathbf{T}}$	vector of mean temperatures in the z direction, K
T^*	reference temperature, K
T_0	initial temperature, K
t	time, s
t_1	starting time for the heat flux application, s
$\mathbf{v}$	observation model noise vector
$\mathbf{w}$	evolution model noise vector
x	spatial independent variable, m
x_1	lower boundary for the proposed heat flux in the x direction, m
x_2	upper boundary for the proposed heat flux in the x direction, m
$\mathbf{x}$	state vector
$\hat{\mathbf{x}}_n$	posterior estimate of the state vector
$\hat{\mathbf{x}}_{n\|n-1}$	prior estimate of the state vector
y	spatial independent variable, m
y_1	lower boundary for the proposed heat flux in the y direction, m
y_2	upper boundary for the proposed heat flux in the y direction, m
$\mathbf{y}$	observation vector
z	spatial independent variable, m
Δt	time step, s
Δx	finite-volume grid spacing in the x direction, m
Δy	finite-volume grid spacing in the y direction, m
Δz	finite-volume grid spacing in the z direction, m
$\boldsymbol{\varepsilon}$	approximation error of the state vector
$\boldsymbol{\zeta}$	approximation error of the observation vector
π	probability density function
σ_q	standard deviation for the random walk process, W/m^2
σ_t	standard deviation of the mean temperatures on the reduced model, K
σ_y	standard deviation of the simulated measurements, K
$\boldsymbol{\omega}$	standard Gaussian random vector
AEM	Approximation Error Model
CEM	Complete Error Model
CLSA	Classical Lumped System Analysis
EEM	Enhanced Error Model
ILSA	Improved Lumped System Analysis
KF	Kalman Filter
MAP	Maximum A Posteriori

[3], Laplace's Transform [4], and the DCT/Laplace Method [5]. Other inverse heat transfer problems of interest can be found in references [6–14]. The main contribution of this paper is to show that the nonlinear inverse problem can be solved by combining the classical Kalman Filter (KF) [15–19], a Lumped System Analysis [20], and the Approximation Error Model (AEM) [1, 21, 22]. The KF is capable of estimating the instantaneous state of a linear dynamic system perturbed by Gaussian white noise, using measurements linearly related to this state and also corrupted by Gaussian white noise [17]. To provide a linear dynamic system to the KF, a Lumped

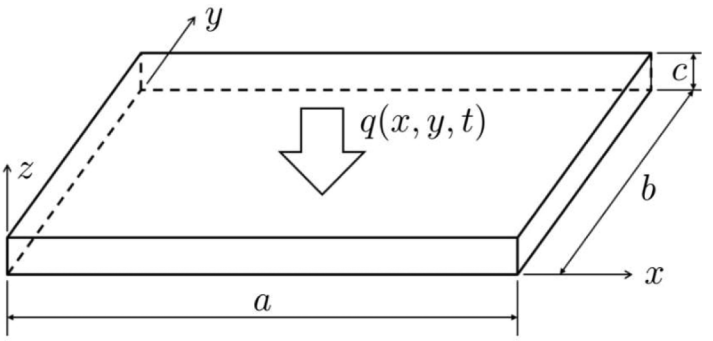

Figure 1. Geometry of the physical problem.

System Analysis was used in this work to simplify the original nonlinear three-dimensional model by transforming it into a two-dimensional linear problem. The AEM then allows one to quantify the modeling errors of the reduced model in comparison to the original one, in order to improve the accuracy of the estimates [21]. Several studies have been carried out, showing the efficacy of the Lumped System Analysis [20, 23] and of the KF [15, 17–19]. Similarly for the AEM, papers can be found in the literature where such an approach has been used with the Metropolis–Hastings algorithm, providing excellent estimates at reduced computational costs [1, 24]. Recently, it has been shown that the classical KF can be used in conjunction with the AEM, by redefining the evolution–observation models to account for the state and observation approximation errors [22]. The approach proposed in this paper is capable of sequentially estimating a boundary heat flux at low computational costs, as described next.

FORWARD PROBLEM

The physical problem considered here involves the application of a high-magnitude heat flux at the top surface of a flat plate, while temperature measurements are taken at its bottom surface, as shown in Figure 1. The dimensions of the flat plate are given by Table 1. Since the focus is on fast transients that take place at short times, the bottom and lateral surfaces are considered as thermally insulated. The heat flux is location- and time dependent and the initial temperature distribution is considered to be uniform. Based on these assumptions, the resulting mathematical model, named here as complete model, is given by [23]

Table 1. Dimensions of the flat plate

Dimension	Value [mm]
a	120
b	120
c	3

$$C(T_c)\frac{\partial T_c}{\partial t} = \frac{\partial}{\partial x}\left[k_T(T_c)\frac{\partial T_c}{\partial x}\right] + \frac{\partial}{\partial y}\left[k_T(T_c)\frac{\partial T_c}{\partial y}\right] + \frac{\partial}{\partial z}\left[k_T(T_c)\frac{\partial T_c}{\partial z}\right]$$
$$\text{in } 0 < x < a,\ 0 < y < b,\ 0 < z < c,\ t > 0 \tag{1.a}$$

$$\frac{\partial T_c}{\partial x} = 0 \quad \text{at} \quad x = 0 \quad \text{and} \quad x = a,\ 0 < y < b,\ 0 < z < c,\ t > 0 \tag{1.b}$$

$$\frac{\partial T_c}{\partial y} = 0 \quad \text{at} \quad y = 0 \quad \text{and} \quad y = b,\ 0 < x < a,\ 0 < z < c,\ t > 0 \tag{1.c}$$

$$\frac{\partial T_c}{\partial z} = 0 \quad \text{at} \quad z = 0,\ 0 < x < a,\ 0 < y < b,\ t > 0 \tag{1.d}$$

$$k_T(T_c)\frac{\partial T_c}{\partial z} = q(x,y,t) \quad \text{at} \quad z = c,\ 0 < x < a,\ 0 < y < b,\ t > 0 \tag{1.e}$$

$$T_c = T_0 \quad \text{at} \quad t = 0,\ \text{in } 0 \le x \le a,\ 0 \le y \le b,\ 0 \le z \le c \tag{1.f}$$

The selected material for this work is stainless steel. The thermal properties are modeled as functions of temperature in the form [25]

$$C(T) = 1324.75T + 3557900\ [\mathrm{J/m^3K}] \tag{2.a}$$

$$k_T(T) = 12.45 + 0.014\ T + 2.517 \times 10^{-6}T^2\ [\mathrm{W/mK}] \tag{2.b}$$

The proposed inverse problem cannot be solved with KF, since the complete model is nonlinear. Regarding other techniques, a similar inverse problem solved with the complete model, using the Metropolis–Hastings algorithm in a time range of 2.0 seconds with $\Delta x = \Delta y = 5\,\mathrm{mm}$, $\Delta z = 0.5\,\mathrm{mm}$, $\Delta t = 0.01\,\mathrm{s}$, and 10^5 states of the Markov chain, led to eight days of computational time [1]. In order to reduce this extremely high computational cost, a simpler model should be considered. The reduced model used in this work was then obtained by applying the steps described next [1].

1st Step: Linearization of the Complete Model

The first step involves the linearization of problem (1.a–f) by substituting the temperature-dependent thermal properties by constant thermal properties C^* and k_T^*, which are obtained by evaluating Eqs. (2.a) and (2.b) at a reference temperature of $T^* = 600$ K [1], that is,

$$C^* = C(T^*) \tag{3.a}$$
$$k_T^* = k_T(T^*) \tag{3.b}$$

2nd Step: Lowering of the Number of Dimensions

The discrete solution of a three-dimensional problem generally leads to large memory requirements and computational costs. Thus, methodologies for appropriately lowering the number of dimensions of the forward problem are desired. One possible approach for the present case is to perform the analysis in terms of the mean temperature in the z direction, which is defined as

$$\overline{T}(x,y,t) = \frac{1}{c}\int_0^c T(x,y,z,t)dz \tag{4}$$

The application of the operator that defines this mean temperature to the linearized version of Eq. (1.a) is straightforward. The resulting expression for the diffusion term in the z direction is the difference of the heat fluxes at the $z=c$ and $z=0$ surfaces of the plate, that is,

$$\frac{1}{c}\int_0^c \frac{\partial}{\partial z}\left[k_T^* \frac{\partial T}{\partial z}\right]dz = \frac{q(x,y,t)}{c} \tag{5}$$

The operator of mean temperature in the z direction is also applied to the linearized versions of Eqs. (1.b), (1.c), and (1.f). The final result is the following linear and two-dimensional reduced model:

$$C^* \frac{\partial \overline{T}(x,y,t)}{\partial t} = k_T^* \frac{\partial^2 \overline{T}}{\partial x^2} + k_T^* \frac{\partial^2 \overline{T}}{\partial y^2} + \frac{q(x,y,t)}{c} \text{ in } 0 < x < a,\ 0 < y < b,\ t > 0 \tag{6.a}$$

$$\frac{\partial \overline{T}}{\partial x} = 0 \quad \text{at} \quad x = 0 \quad \text{and } x = a,\ 0 < y < b,\ t > 0 \tag{6.b}$$

$$\frac{\partial \overline{T}}{\partial y} = 0 \quad \text{at} \quad y = 0 \quad \text{and} \quad y = b,\ 0 < x < a,\ t > 0 \tag{6.c}$$

$$\overline{T} = T_0 \quad \text{at} \quad t = 0,\ \text{in } 0 \le x \le a,\ 0 \le y \le b \tag{6.d}$$

3rd Step: The Lumped System Analysis

Compared with the complete model, the reduced model is much simpler and its solution can be found at much lower computational costs. Moreover, its use as a forward model allows the application of the KF to solve the inverse problem. However, the solution of this mathematical problem provides the mean temperature in the z direction instead of the temperatures at the plate surfaces. Such temperatures can be approximately related through the Lumped System Analysis [20]. In the Classical Lumped System Analysis (CLSA), the temperature gradients in the z direction are

neglected. Thus, the temperature at the plate surfaces can be approximated by the mean temperature in the z direction, obtained by solving the reduced model. In the so-called Improved Lumped System Analysis (ILSA), the temperature gradient in the z direction is not neglected, but approximately taken into account using the following Hermite's formulas for integrals [20]:

$$\int_0^h y(x)dx = \frac{h}{2}[y(0) + y(h)] + O(h^3) \tag{7.a}$$

$$\int_0^h y(x)dx = \frac{h}{2}[y(0) + y(h)] + \frac{h^2}{12}\left[\left.\frac{dy}{dx}\right|_{x=0} - \left.\frac{dy}{dx}\right|_{x=h}\right] + O(h^5) \tag{7.b}$$

Equation (7.a) is used to approximate the integral of the temperature gradient in the z direction, while Eq. (7.b) is used to approximate the mean temperature in the z direction, thus leading to the following approximations for the temperatures at the $z = 0$ and $z = c$ surfaces of the plate in terms of the solution of the reduced model [1]:

$$T(x, y, 0, t) \approx \overline{T}(x, y, t) - \frac{c}{6k_T^*} q(x, y, t) \tag{8.a}$$

$$T(x, y, c, t) \approx \overline{T}(x, y, t) + \frac{c}{3k_T^*} q(x, y, t) \tag{8.b}$$

INVERSE PROBLEM

The proposed inverse problem of estimating the unsteady heat flux distribution at $z = c$ is solved with a Bayesian filter, where the probability distribution of the unknown state vector $\mathbf{x}_n$, given the set of observations $\mathbf{y}_{0:n}$, is built with Bayes' theorem. The complete characterization of this posterior probability distribution function allows for statistical inference about the unknowns [15].

The KF is the most widely used Bayesian filtering method [21], but it can be applied only to linear problems with Gaussian joint probability function $\pi(\mathbf{x}, \mathbf{y})$, in the form of an evolution–observation model such as

$$\mathbf{x}_n = \mathbf{F}_n \mathbf{x}_{n-1} + \mathbf{w}_n \tag{9.a}$$

$$\mathbf{y}_n = \mathbf{H}_n \mathbf{x}_n + \mathbf{v}_n \tag{9.b}$$

where $\mathbf{w}_n$ and $\mathbf{v}_n$ are Gaussian random vectors with zero means and covariance matrices $\mathbf{Q}_n$ and $\mathbf{R}_n$, respectively.

The state vector $\mathbf{x}_n$ is presented in Eq. (10), where $\overline{\mathbf{T}}_n$ contains the values of mean temperature in the z direction at the center of each control volume of the numerical grid along the (x,y) plane, while $\mathbf{q}_n$ contains the heat flux values at the same locations, at each time t_n. The observations $\mathbf{y}_n$ used for the estimation of

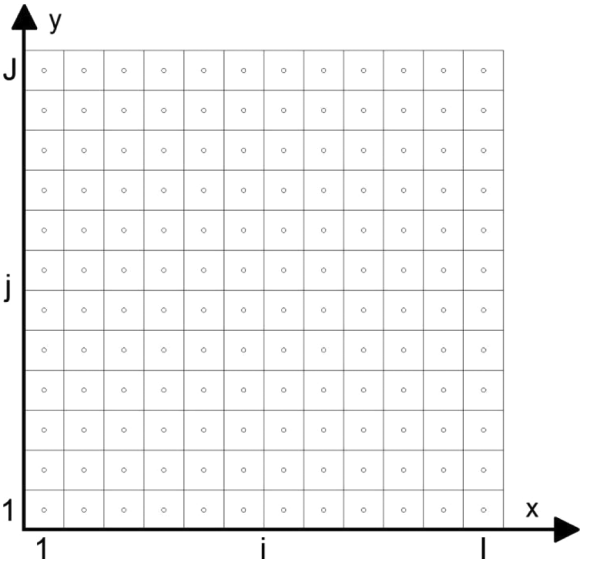

Figure 2. Example of a finite-volume uniform grid with I volumes in the x direction and J volumes in the y direction.

the state vector $\mathbf{x}_n$ are given by the measured temperatures at the surface $z = 0$, at the center of the same control volumes used for $\overline{\mathbf{T}}_n$ and $\mathbf{q}_n$. In the example of the grid illustrated in Figure 2, containing I volumes in the x direction and J volumes in the y direction, the total number of unknowns in $\mathbf{x}_n$ is thus $2IJ$.

$$\mathbf{x}_n = \begin{bmatrix} \overline{\mathbf{T}}_n \\ \mathbf{q}_n \end{bmatrix} \tag{10}$$

The $\mathbf{F}_n$ matrix, with size $2IJ \times 2IJ$, is built by joining four smaller matrices of size $IJ \times IJ$, that is,

$$\mathbf{F}_n = \begin{bmatrix} \mathbf{A}_n & \mathbf{B}_n \\ \mathbf{0} & \mathbf{I} \end{bmatrix} \tag{11}$$

where $\mathbf{A}_n$ and $\mathbf{B}_n$ are matrices that result from the discretization of the reduced model. While $\mathbf{A}_n$ accounts for heat diffusion in the domain, the $\mathbf{B}_n$ matrix considers the effect of heat flux on the temperatures. The $\mathbf{0}$ and $\mathbf{I}$ matrices correspond to a matrix with zero elements and the identity matrix, respectively, both with sizes $IJ \times IJ$. They result from a random walk model used for the evolution of the heat flux, in the form

$$\mathbf{q}_n = \mathbf{q}_{n-1} + \sigma_q \boldsymbol{\omega} \tag{12}$$

where $\boldsymbol{\omega}$ is a Gaussian vector with zero mean and identity covariance matrix, while the standard deviation of the random walk is denoted by σ_q.

The $\mathbf{H}_n$ matrix of the observation model is of size $IJ \times 2IJ$ and is also built by combining two matrices of size $IJ \times IJ$:

$$\mathbf{H}_n = [\mathbf{I} \quad \mathbf{C}] \tag{13}$$

The $\mathbf{C}$ matrix depends on whether the measurement model is based on the CLSA or on the ILSA, that is,

$$\mathbf{C} = \mathbf{0} \quad \text{for CLSA} \tag{14.a}$$

$$\mathbf{C} = -\frac{c}{6k_T^*}\mathbf{I} \quad \text{for ILSA} \tag{14.b}$$

The recursive equations of the KF are given by [17–19, 21]:

$$\widehat{\mathbf{x}}_{n|n-1} = \mathbf{F}_n \widehat{\mathbf{x}}_{n-1} \tag{15.a}$$

$$\mathbf{P}_{n|n-1} = \mathbf{F}_n \mathbf{P}_{n-1} \mathbf{F}_n^T + \mathbf{Q}_n \tag{15.b}$$

$$\mathbf{K}_n = \mathbf{P}_{n|n-1} \mathbf{H}_n^T (\mathbf{H}_n \mathbf{P}_{n|n-1} \mathbf{H}_n^T + \mathbf{R}_n)^{-1} \tag{15.c}$$

$$\widehat{\mathbf{x}}_n = \widehat{\mathbf{x}}_{n|n-1} + \mathbf{K}_n (\mathbf{y}_n - \mathbf{H}_n \widehat{\mathbf{x}}_{n|n-1}) \tag{15.d}$$

$$\mathbf{P}_n = (\mathbf{I} - \mathbf{K}_n \mathbf{H}_n) \mathbf{P}_{n|n-1} \tag{15.e}$$

We note that these equations do not account for modeling errors, for example, such as those resulting from the use of the reduced model given by Eqs. (6.a–d), instead of the complete model given by Eqs. (1.a–f). The AEM, developed by Kaipio and coworkers [21, 22], can be conveniently used within the Bayesian framework, for taking such errors into account, as described next.

AEM

For the solution of a state estimation problem, extremely accurate evolution and observation models, which are supposed to perfectly represent the physical phenomena, would possibly be considered if their numerical solution could be calculated within a feasible computational time. Here we write such models in terms of general nonlinear functions, respectively, as [19, 21]

$$\mathbf{x}_n = \mathbf{f}^*(\mathbf{x}_{n-1}, \ \mathbf{w}_n^*) \tag{16.a}$$

$$\mathbf{y}_n = \mathbf{g}^*(\mathbf{x}_n, \ \mathbf{v}_n^*) \tag{16.b}$$

On the other hand, if the computational times are too large for the use of the complete models given by Eqs. (16.a,b), such as in this work, a reduced evolution model, $\mathbf{f}(\mathbf{x}_{n-1}, \mathbf{w}_n)$, and a reduced observation model, $\mathbf{g}(\mathbf{x}_n, \mathbf{v}_n)$, could be considered for the inverse analysis. The solution of the state estimation problem with the reduced models is faster, but errors between the complete and reduced models must

be taken into account in the analysis. By adding and subtracting $\mathbf{f}(\mathbf{x}_{n-1}, \mathbf{w}_n)$ to Eq. (16.a) and $\mathbf{g}(\mathbf{x}_n, \mathbf{v}_n)$ to Eq. (16.b), we can write

$$\mathbf{x}_n = \mathbf{f}(\mathbf{x}_{n-1}, \mathbf{w}_n) + [\mathbf{f}^*(\mathbf{x}_{n-1}, \mathbf{w}_n^*) - \mathbf{f}(\mathbf{x}_{n-1}, \mathbf{w}_n)] \tag{17.a}$$

$$\mathbf{y}_n = \mathbf{g}(\mathbf{x}_n, \mathbf{v}_n) + [\mathbf{g}^*(\mathbf{x}_n, \mathbf{v}_n^*) - \mathbf{g}(\mathbf{x}_n, \mathbf{v}_n)] \tag{17.b}$$

or alternatively,

$$\mathbf{x}_n = \mathbf{f}(\mathbf{x}_{n-1}, \mathbf{w}_n) + \boldsymbol{\varepsilon}_n \tag{18.a}$$

$$\mathbf{y}_n = \mathbf{g}(\mathbf{x}_n, \mathbf{v}_n) + \boldsymbol{\zeta}_n \tag{18.b}$$

where $\boldsymbol{\varepsilon}_n = [\mathbf{f}^*(\mathbf{x}_{n-1}, \mathbf{w}_n^*) - \mathbf{f}(\mathbf{x}_{n-1}, \mathbf{w}_n)]$ and $\boldsymbol{\zeta}_n = [\mathbf{g}^*(\mathbf{x}_n, \mathbf{v}_n^*) - \mathbf{g}(\mathbf{x}_n, \mathbf{v}_n)]$ are the approximation errors for the evolution and observations models, respectively [21].

In order to develop the AEM, one can assume, for example, $\text{cov}(\mathbf{x}_n, \boldsymbol{\varepsilon}_n) = \text{cov}(\mathbf{x}_n, \boldsymbol{\zeta}_n) = 0$, that is, the sought state variables and the approximation errors are independent, which is usually referred to as the Enhanced Error Model (EEM) [1, 21, 22]. Based on our previous experience and excellent results obtained for the solution of a similar inverse problem with the Markov chain Monte Carlo method [1], the EEM is used in this paper. For the application of the EEM to the linear state estimation problem of this work, the evolution and observation models given by Eqs. (18.a,b) are then rewritten as

$$\mathbf{x}_n = \mathbf{F}_n \mathbf{x}_{n-1} + \mathbf{w}_n + \boldsymbol{\varepsilon}_n \tag{19.a}$$

$$\mathbf{y}_n = \mathbf{H}_n \mathbf{x}_n + \mathbf{v}_n + \boldsymbol{\zeta}_n \tag{19.b}$$

and the recursive equations of the KF become [22]

$$\widehat{\mathbf{x}}_{n|n-1} = \mathbf{F}_n \widehat{\mathbf{x}}_{n-1} + \text{E}(\boldsymbol{\varepsilon}_n) \tag{20.a}$$

$$\mathbf{P}_{n|n-1} = \mathbf{F}_n \mathbf{P}_{n-1} \mathbf{F}_n^T + \mathbf{Q}_n + \text{cov}(\boldsymbol{\varepsilon}_n) \tag{20.b}$$

$$\mathbf{K}_n = \mathbf{P}_{n|n-1} \mathbf{H}_n^T [\mathbf{H}_n \mathbf{P}_{n|n-1} \mathbf{H}_n^T + \text{cov}(\boldsymbol{\zeta}_n) + \mathbf{R}_n]^{-1} \tag{20.c}$$

$$\widehat{\mathbf{x}}_n = \widehat{\mathbf{x}}_{n|n-1} + \mathbf{K}_n [\mathbf{y}_n - \mathbf{H}_n \widehat{\mathbf{x}}_{n|n-1} - \text{E}(\boldsymbol{\zeta}_n)] \tag{20.d}$$

$$\mathbf{P}_n = (\mathbf{I} - \mathbf{K}_n \mathbf{H}_n) \mathbf{P}_{n|n-1} \tag{20.e}$$

Therefore, for the proper application of the recursive Eqs. (20.a–e) of the KF that take into account the modeling errors, the statistics of such errors must be quantified. In this work the approximation error statistics are calculated online, that is, during the estimation process, by sequentially calculating the system's state variables with both the reduced and the complete models. In order to allow the computation of the statistics, the state variables are sampled from the Gaussian distributions that result from the application of the KF given by Eq. (20.a–e). The estimators of the statistics with M samples are obtained from [22]

$$\mathrm{E}(\boldsymbol{\varepsilon}_n) = \frac{1}{M}\sum_{i=1}^{M} \boldsymbol{\varepsilon}_{i,n} \tag{21.a}$$

$$\mathrm{E}(\boldsymbol{\zeta}_n) = \frac{1}{M}\sum_{i=1}^{M} \boldsymbol{\zeta}_{i,n} \tag{21.b}$$

$$\mathrm{cov}(\boldsymbol{\varepsilon}_n) = \frac{1}{M-1}\sum_{i=1}^{M} [\boldsymbol{\varepsilon}_{i,n} - \mathrm{E}(\boldsymbol{\varepsilon}_n)][\boldsymbol{\varepsilon}_{i,n} - \mathrm{E}(\boldsymbol{\varepsilon}_n)]^T \tag{21.c}$$

$$\mathrm{cov}(\boldsymbol{\zeta}_n) = \frac{1}{M-1}\sum_{i=1}^{M} [\boldsymbol{\zeta}_{i,n} - \mathrm{E}(\boldsymbol{\zeta}_n)][\boldsymbol{\zeta}_{i,n} - \mathrm{E}(\boldsymbol{\zeta}_n)]^T \tag{21.d}$$

Note that, in this work, the calculation of the modeling error statistics require the coupling between the linear two-dimensional reduced model given by Eqs. (6.a–d) and the nonlinear three-dimensional complete model given by Eqs. (1.a–f). For the sequential calculation of the approximation error, the complete model is solved with the implicit finite-volume method on a grid with three volumes in the z direction at each point (x_i, y_j), as illustrated by Figure 3. In this case, the mean temperature in the z direction can be approximated as an arithmetic mean, while the surface temperatures can be approximated using second-order forward and backward finite differences, respectively, given by

$$\overline{T}(x_i, y_j, t) = \frac{1}{3}[T_1(x_i, y_j, t) + T_2(x_i, y_j, t) + T_3(x_i, y_j, t)] \tag{22.a}$$

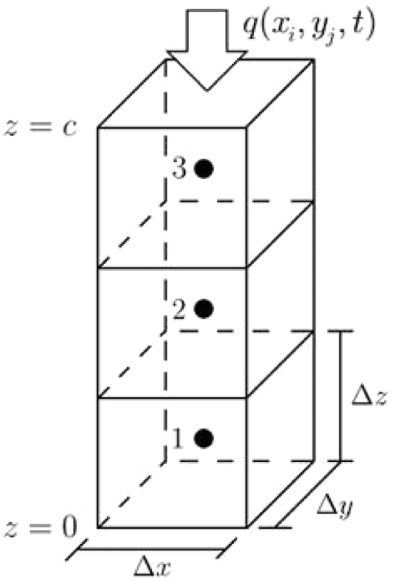

Figure 3. Discretization in the z direction at a (x_i, y_j) point of the complete model grid.

$$T(x_i, y_j, 0, t) \equiv T_{bottom}(x_i, y_j, t) = \frac{1}{8}[9T_1(x_i, y_j, t) - T_2(x_i, y_j, t)] \tag{22.b}$$

$$T(x_i, y_j, c, t) \equiv T_{top}(x_i, y_j, t) = \frac{1}{8}\left[9T_3(x_i, y_j, t) - T_2(x_i, y_j, t) + \frac{3q(x_i, y_j, t)\Delta z}{k_T[T_{top}(x_i, y_j, t)]}\right] \tag{22.c}$$

Equations (22.a–c) are rewritten for the temperature at each of the three points of the numerical grid in the z direction of the complete model as

$$T_1(x_i, y_j, t) = \frac{1}{99}\left[\begin{array}{l} 80T_{bottom}(x_i, y_j, t) + 27\overline{T}(x_i, y_j, t) - 8T_{top}(x_i, y_j, t) \\ + \dfrac{3q(x_i, y_j, t)\Delta z}{k_T[T_{top}(x_i, y_j, t)]} \end{array}\right] \tag{23.a}$$

$$T_2(x_i, y_j, t) = \frac{1}{11}\left[\begin{array}{l} -8T_{bottom}(x_i, y_j, t) + 27\overline{T}(x_i, y_j, t) - 8T_{top}(x_i, y_j, t) \\ + \dfrac{3q(x_i, y_j, t)\Delta z}{k_T[T_{top}(x_i, y_j, t)]} \end{array}\right] \tag{23.b}$$

$$T_3(x_i, y_j, t) = \frac{1}{99}\left[\begin{array}{l} -8T_{bottom}(x_i, y_j, t) + 27\overline{T}(x_i, y_j, t) + 80T_{top}(x_i, y_j, t) \\ - \dfrac{30q(x_i, y_j, t)\Delta z}{k_T[T_{top}(x_i, y_j, t)]} \end{array}\right] \tag{23.c}$$

Hence, the estimated variables $\overline{T}(x_i, y_j, t)$ and $q(x_i, y_j, t)$, obtained with the KF by using the reduced model at each time instant (see Eqs. 20.a–e), are used to generate the temperatures across the plate given by Eqs. (23.a–c), which are required to advance the three-dimensional complete model and then allow the sequential estimation of the approximation error.

RESULTS AND DISCUSSIONS

In this work, the proposed inverse problem was solved using simulated measurements obtained from the solution of the complete model with a reference heat flux, on a sufficiently fine grid. This was done so that the simulated measurements and the estimates from the inverse problem are obtained using different mathematical models and different grid sizes, ensuring that these results are not affected by inverse crimes [21]. The complete model was solved with the implicit scheme of the finite-volume method, while the reduced model was solved with the explicit scheme of the finite-volume method [26–28]. The measurement errors were modeled as mutually uncorrelated and with a constant standard deviation, σ_y. Thus, to simulate the noisy data, a Gaussian vector with zero mean and covariance matrix $\sigma_y^2\mathbf{I}$ was added to the temperatures obtained from the solution of the complete model, where $\mathbf{I}$ stands for the identity matrix. The measurements were simulated by solving the complete model on a grid with $768 \times 768 \times 64$ volumes and a time step of $\Delta t = 10^{-4}$s. The inverse problem was solved on a 24×24 grid with a time step of $\Delta t = 10^{-2}$s.

Table 2. Parameters used for the simulated heat flux from Eq. (24)

Variable	Value
x_1	60 mm
x_2	72 mm
y_1	60 mm
y_2	72 mm
q_0	10^7 W/m^2
t_1	0.4 s

The initial temperature was considered as 300 K. In a real case, surface temperature measurements could be obtained using modern infrared cameras, with standard deviations of the order of 0.01°C [1]. On the other hand, for challenging the performance of the approach proposed in this paper, based on the KF and the EEM, a much higher value for this standard deviation was selected ($\sigma_y = 1$°C). The number of samples used for calculating the approximation errors was $M = 10$. The standard deviation of the random walk model for the evolution of the heat flux was 5×10^4 W/m^2, while the standard deviation of the evolution model for the temperatures was 1°C.

The proposed heat flux to be estimated follows Eq. (24), and its parameters are given in Table 2. The size of the region of application was chosen so it does not necessarily coincide with the coarse grid.

$$q(x, y, t) = \begin{cases} q_0 & \text{if} \quad x_1 \leq x \leq x_2, \quad y_1 \leq y \leq y_2 \quad \text{and} \quad t \geq t_1 \\ 0 & \text{otherwise} \end{cases} \tag{24}$$

The exact values of the temperatures calculated with the complete model at time $t = 2.0$ s are shown in Figure 4. These values are projected on the coarse grid

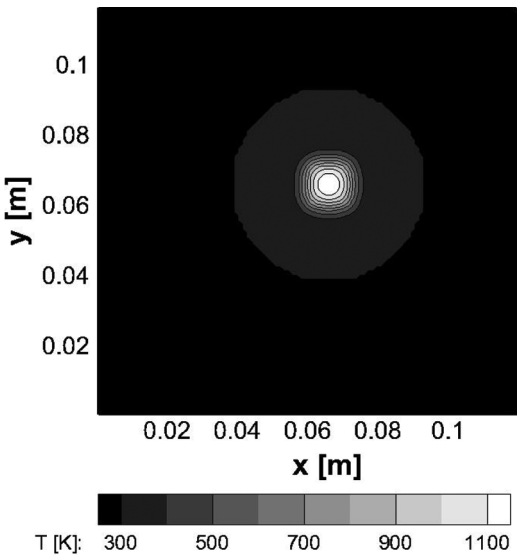

Figure 4. Exact surface temperatures at $z = 0$ and $t = 2.0$ s on the fine grid.

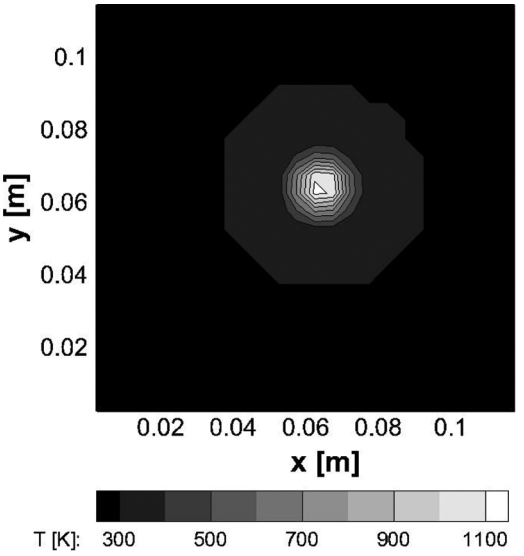

Figure 5. Projection of the exact temperatures on the coarse grid used to solve the inverse problem at $z = 0$ and $t = 2.0$ s.

of the reduced model, resulting in the temperature field shown in Figure 5 at time $t = 2.0$ s. These projected temperature values corrupted with Gaussian noise are then used to solve the inverse problem. The exact heat flux at time $t = 2.0$ s is presented for the fine and coarse grids in Figures 6 and 7, respectively.

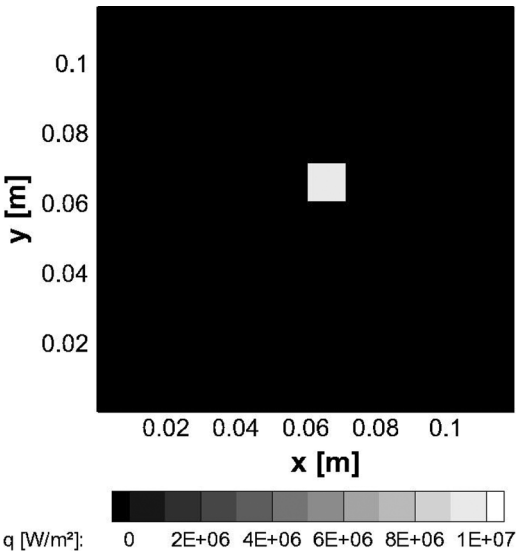

Figure 6. Exact heat flux on the fine grid at time $t = 2.0$ s.

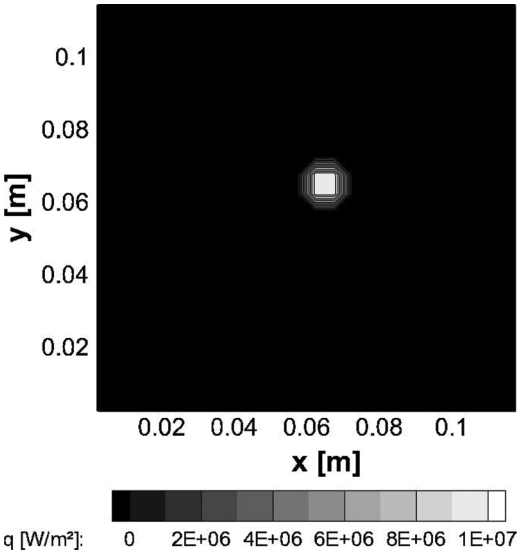

Figure 7. Projection of the exact heat flux on the coarse grid at time $t = 2.0$ s.

The results obtained with the CLSA for the temperature field are presented in Figure 8, while the estimated heat fluxes are presented in Figure 9, at time $t = 2.0$ s. The time evolutions of temperature and heat flux at the point $(x, y, z) = (6.25, 6.25, 0.00)$ cm, which is located inside the region of application of the heat flux where the greatest variations are expected, are presented by Figures 10 and 11, respectively.

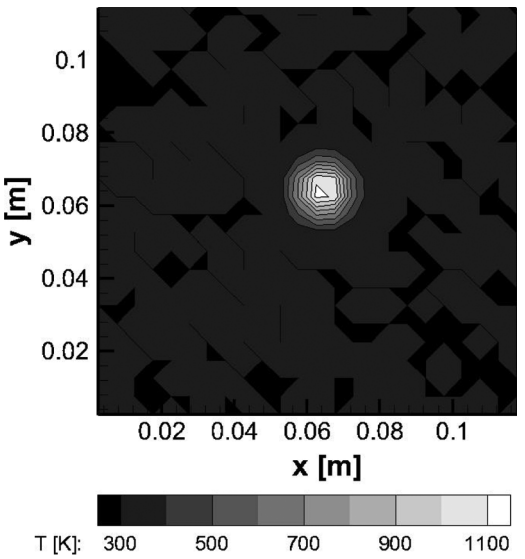

Figure 8. Estimated temperature field at time $t = 2.0$ s using the CLSA.

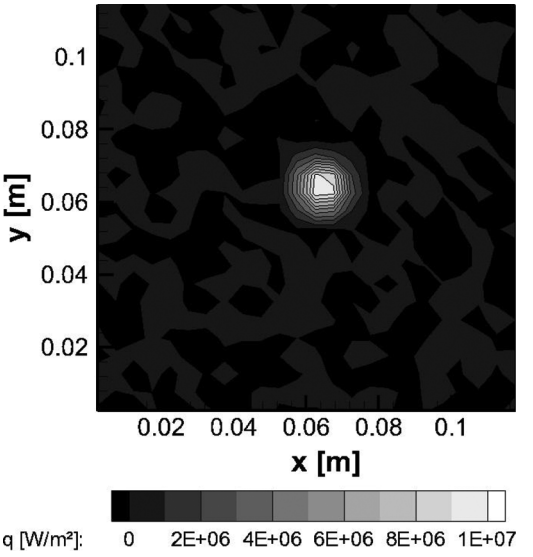

Figure 9. Estimated heat flux at time $t = 2.0$ s using the CLSA.

The results presented in Figure 10 show excellent agreement between the exact and estimated temperatures. The results for the heat flux presented in Figures 9 and 11 show that the EEM successfully compensates for the approximation errors present in the reduced model, thus resulting in a very good agreement between the estimated

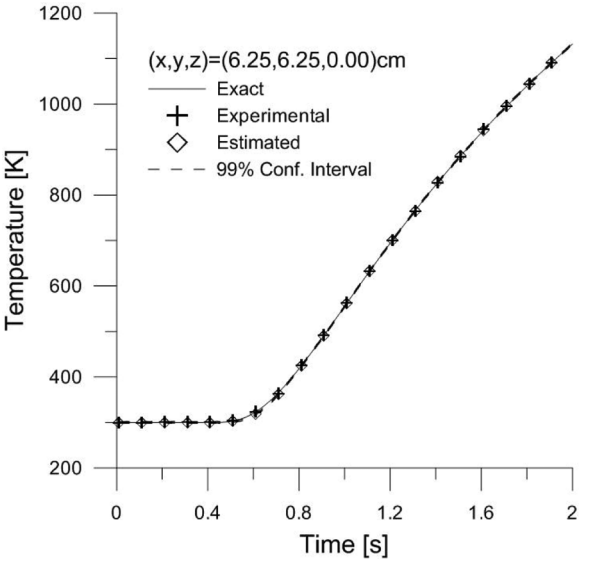

Figure 10. Evolution in time of the reference and estimated temperatures with CLSA at $(x, y, z) = (6.25, 6.25, 0.00)$ cm.

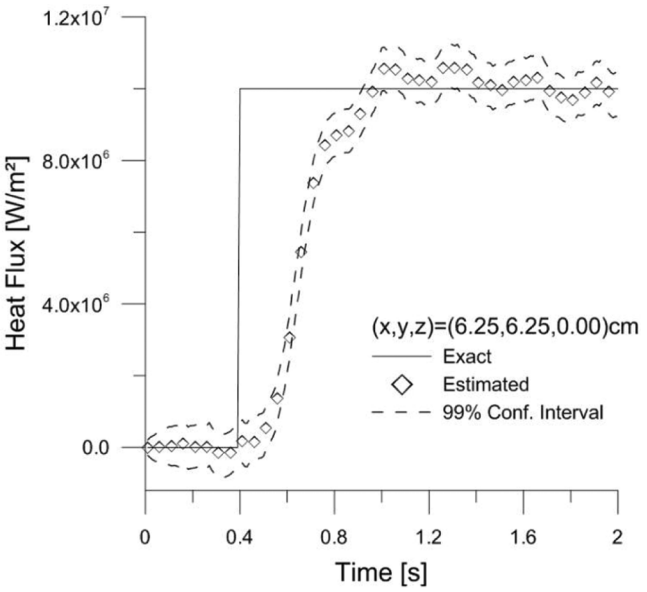

Figure 11. Evolution in time of the reference and estimated heat flux with CLSA at $(x, y, z) = (6.25, 6.25, 0.00)$ cm.

and exact heat fluxes. The temperature residuals at point $(x, y, z) = (6.25, 6.25, 0.00)$cm are not correlated, as shown by Figure 12, despite the fact that the inverse problem was solved with the reduced model. In fact, Figure 13 shows the residual

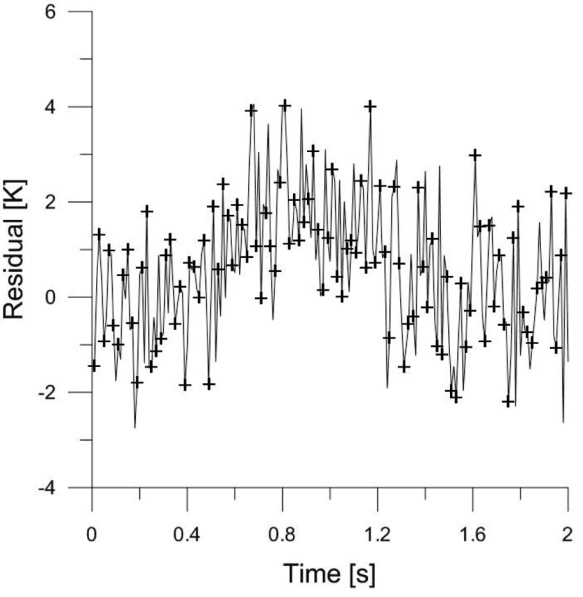

Figure 12. Evolution in time of the residuals at $(x, y, z) = (6.25, 6.25, 0.00)$ cm using the CLSA.

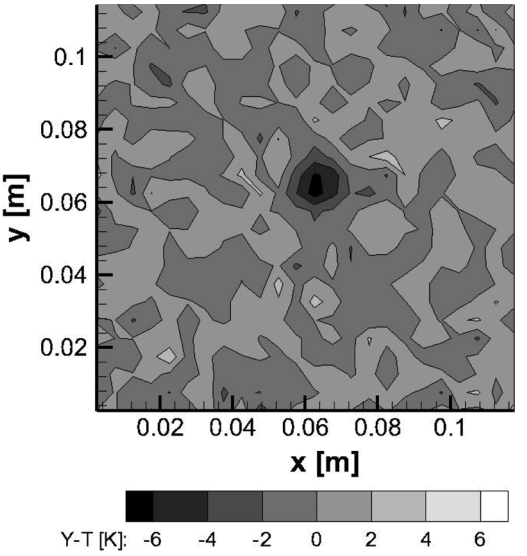

Figure 13. Residuals at time $t = 1.0$ s obtained using the CLSA.

field at time $t = 1.0$ s, which reveals an excellent agreement between estimated and measured temperatures in the whole region.

We now focus our analysis on the results obtained with the ILSA. The estimated temperature field at $t = 2.0$ s is presented in Figure 14. Similarly, Figure 15 presents the estimated heat flux at $t = 2.0$ s. These figures reveal that the

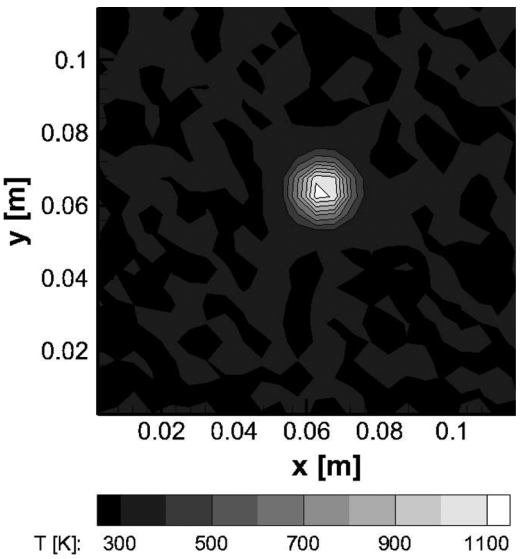

Figure 14. Estimated temperature field using the ILSA at time $t = 2.0$ s.

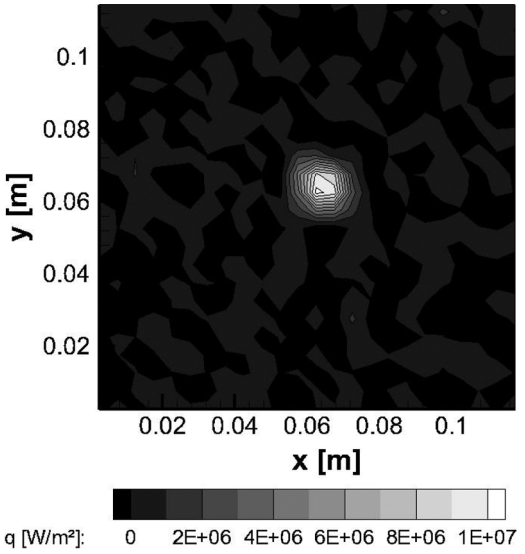

Figure 15. Estimated heat flux field using the ILSA at time $t = 2.0$ s.

state variables can be quite accurately estimated (see also Figures 4–7). A comparison of the time evolution of the estimated state variables with their exact values is also done for point $(x, y, z) = (6.25, 6.25, 0.00)$ cm, in Figures 16 and 17. The results obtained for temperature, presented in Figure 16, show an excellent agreement

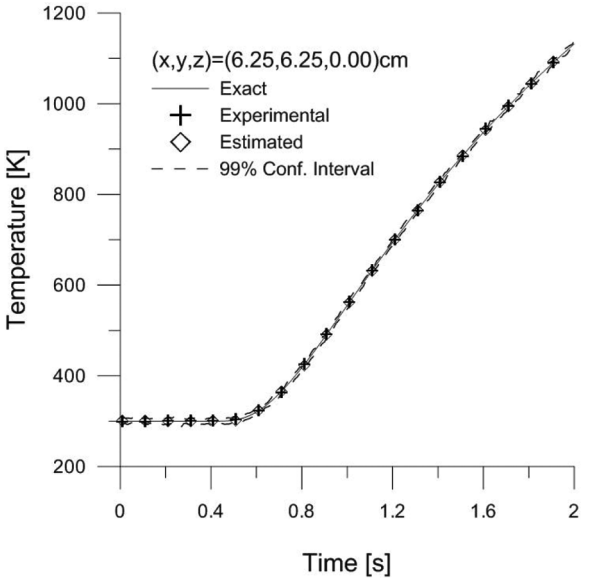

Figure 16. Evolution in time of the reference and estimated temperatures with ILSA at $(x, y) = (6.25, 6.25, 0.00)$ cm.

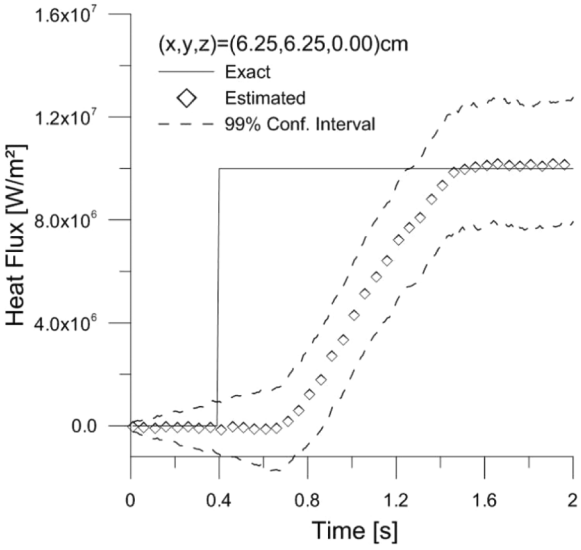

Figure 17. Evolution in time of the reference and estimated heat flux with ILSA at $(x, y) = (6.25, 6.25, 0.00)$ cm.

between the exact and estimated values, but with slightly larger confidence intervals than for the case with CLSA (see Figure 10). Figure 17 shows that the transient variation of the heat flux can be quite accurately estimated, although larger confidence

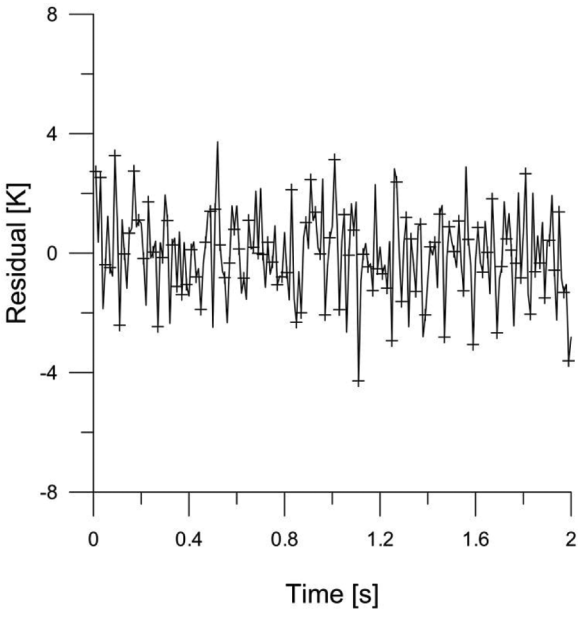

Figure 18. Evolution in time of the residuals at $(x, y, z) = (6.25, 6.25, 0.00)$ cm, obtained using the ILSA.

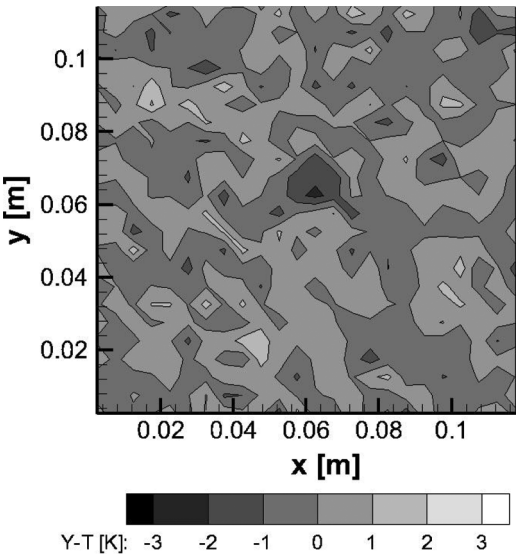

Figure 19. Residuals at time $t = 1.0$ s, obtained using the ILSA.

intervals and a larger time lag are noticed, compared with the case with the CLSA (see Figure 11). On the other hand, the time variation of the heat flux estimated with the ILSA was smoother than that estimated with the CLSA. This behavior was due to the standard deviation of the random walk model for heat flux, which was the same for both cases. The analysis of the residuals, with transient variation for the point (x, y, z) = (6.25, 6.25, 0.00)cm presented by Figure 18 and with spatial distribution at $t = 1.0$ s presented by Figure 19, shows that they are uncorrelated. Such is the case despite the fact that the inverse problem was solved with the reduced model.

The results obtained in this paper reveal that the proposed inverse analysis approach is not sensitive to the accuracy of the lumping technique used to obtain the reduced model. While the improved lumped formulation is certainly more accurate than the classical lumped formulation for direct (forward) problem simulations, the EEM was capable of effectively dealing with the approximation errors for these two reduced models.

All the computer codes used in this paper were developed in FORTRAN90 language. The results were obtained on an Intel®Core™ i7-3610QM CPU with 8GB of RAM. The processes of matrix inversion and multiplication of the KF were executed in parallel, by using the OpenMP platform and four threads. On average, each run of the computational code that combines the KF and the EEM took around 5 minutes to be completed.

CONCLUSIONS

This paper presented the inverse problem of estimating a boundary heat flux applied on the top surface of a flat plate by using transient temperature measurements taken on the bottom side of the plate. The heat flux is position and time

dependent and has high magnitude. The inverse problem was solved combining two different Lumped System Analyses: the KF and the AEM. The main contribution here is to show that it is possible to solve complex inverse problems using reduced models, provided that the approximation errors are properly quantified. While the complete model, which is assumed to perfectly reproduce the physics of the problem, is nonlinear and three-dimensional, the reduced model used for the inverse analysis was linear and two-dimensional.

The approximation errors in this paper were sequentially calculated, as the KF was applied to advance the solution in time. Indeed, the EEM, used in this paper for estimating the approximation errors, was capable of accurately identifying the spatial and time variations of the imposed heat flux, resulting in small and practically uncorrelated residuals, despite the fact that the reduced model was used in the inverse analysis instead of the complete model. We note that the proposed approach was also robust with respect to large uncertainties in the evolution and observations models and was not affected by the accuracy of the lumping technique used to obtain the reduced model.

FUNDING

The authors would like to thank the Brazilian agencies for the fostering of science, Conselho Nacional de Desenvolvimento Científico e Tecnológico (CNPq), Coordenação de Aperfeiçoamento de Pessoal de Nível Superior (CAPES), Fundação Carlos Chagas Filho de Amparo à Pesquisa do Estado do Rio de Janeiro (FAPERJ), and Programa de Recursos Humanos da Agência Nacional de Óleo, Gás Natural e Biocombustíveis (UNH) for the financial support for this work.

REFERENCES

1. H. R. B. Orlande, G. S. Dulikravich, M. Neumayer, D. Watzenig, and M. J. Colaço, Accelerated Bayesian Inference for the Estimation of Spatially Varying Heat Flux in a Heat Conduction Problem, *Numer. Heat Transf. Part A*, vol. 65, pp. 1–25, 2013.
2. B. H. Dennis and G. S. Dulikravich, Simultaneous Determination of Steady Temperatures and Heat Fluxes on Surfaces of Three Dimensional Objects Using FEM, ASME IMECE2001/HTD-24310, New York, November 11–16, 2001.
3. B. H. Dennis and G. S. Dulikravich, Inverse Determination of Unsteady Temperatures and Heat Fluxes on Inaccessible Boundaries, *Inverse Ill-Posed Probl.*, vol. 20, no. 5–6, pp. 791–803, 2012.
4. Z. C. Feng, J. K. Chen, Y. Zhang, and J. L. Griggs Jr., Estimation of Front Surface Temperature and Heat Flux of a Locally Heated Plate from Distributed Sensor Data on the Back Surface, *Int. J. Heat Mass Transf.*, vol. 54, pp. 3431–3439, 2011.
5. N. Afrin, Z. C. Feng, Y. Zhang, and J. K. Chen, Inverse Estimation of Front Surface Temperature of a Locally Heated Plate with Temperature-dependent Conductivity via Kirchhoff Transformation, *Int. J. Therm. Sci.*, vol. 69, pp. 53–60, 2013.
6. S. K. Kim, Prameterized Gradient Integration Method For Inverse Heat Conduction Problems, *Numer. Heat Transf. Part B Fundam.*, vol. 61, no. 2, pp. 116–128, 2012.
7. F. Berntsson, An Inverse Heat Conduction Problem and Improving Shielded Thermocouple Accuracy, *Numer. Heat Transf. Part A Appl.*, vol. 61, no. 10, pp. 754–763, 2012.

8. M. R. Golbahar Haghighi, P. Malekzadeh, H. Rahideh, and M. Vaghefi, Inverse Transient Heat Conduction Problems of a Multilayered Functionally Graded Cylinder, *Numer. Heat Transf. Part A Appl.*, vol. 61, no. 9, pp. 717–733, 2012.
9. A. Azimi, K. Bamdad, and H. Ahmadikia, Inverse Hyperbolic Heat Conduction in Fins with Arbitrary Profiles, *Numer. Heat Transf. Part A Appl.*, vol. 61, no. 3, pp. 220–240, 2012.
10. E. Hetmaniok, I. Nowak, D. Słota, and A. Zielonka, Determination of Optimal Parameters for the Immune Algorithm used for Solving Inverse Heat Conduction Problems with and Without a Phase Change, *Numer. Heat Transf. Part B Fundam.*, vol. 62, no. 6, pp. 462–478, 2012.
11. H. Rahideh, P. Malekzadeh, M. R. Golbahar Haghighi, and M. Vaghefi, Two-Dimensional Inverse Transient Heat Conduction Analysis of Laminated Functionally Graded Circular Plates, *Numer. Heat Transf. Part A Appl.*, vol. 62, no. 12, pp. 992–1014, 2012.
12. S. Vakili and M. S. Gadala, A Modified Sequential Particle Swarm Optimization Algorithm with Future Time Data for Solving Transient Inverse Heat Conduction Problems, *Numer. Heat Transf. Part A Appl.*, vol. 59, no. 12, pp. 911–933, 2011.
13. K.-C. Liu and C.-T. Lin, Solution of an Inverse Heat Conduction Problem in a Bi-Layered Spherical Tissue, *Numer. Heat Transf. Part A Appl.*, vol. 58, no. 10, pp. 802–818, 2010.
14. S. K. Kim, Resolving the Final Time Singularity in Gradient Methods for Inverse Heat Conduction Problems, *Numer. Heat Transf. Part B Fundam.*, vol. 57, no. 1, pp. 74–88, 2010.
15. Z. Chen, Bayesian Filtering: from Kalman Filters to Particle Filters, and Beyond, Statistics (Ber), vol. 182, no. 1, pp. 1–69, 2003.
16. D. Gamerman, *Markov Chain Monte Carlo: Stochastic Simulation for Bayesian Inference*, Taylor & Francis, Boca Raton, FL, 1997.
17. M. S. Grewal and A. P. Andrews, *Kalman Filtering: Theory and Practice Using MATLAB*, Wiley, Hoboken, 2008.
18. R. E. Kalman, A New Approach to Linear Filtering and Prediction Problems, *Trans. ASME-Journal Basic Eng.*, vol. 82, no. Series D, pp. 35–45, 1960.
19. H. R. B. Orlande, M. J. Colaço, G. S. Dulikravich, F. L. V. Vianna, W. B. da Silva, H. M. Fonseca, and O. Fudym, State Estimation Problems in Heat Transfer, *Int. J. Uncertain. Quantif.*, vol. 2, no. 3, pp. 239–258, 2012.
20. R. M. Cotta and M. D. Mikhailov, *Heat Conduction: Lumped Analysis, Integral Transforms, Symbolic Computation*, Wiley Ed., Chichester, 1997.
21. J. P. Kaipio and E. Somersalo, Statistical and Computational Inverse Problems. Springer Science+Business Media, Inc, New York, NY, 2004.
22. J. Huttunen and J. P. Kaipio, Approximation and Modelling Errors in Nonstationary Inverse Problems, University of Kuopio, Kuopio University Library, Kuopio, 2008.
23. M. N. Ozisik, *Heat Conduction*, 2nd ed., John Wiley & Sons, Inc., New York, NY, 1993.
24. M. Neumayer, D. Watzenig, H. R. B. Orlande, M. J. Colaço, and G. S. Dulikravich, Fast Bayesian Inference for an Inverse Heat Transfer Problem Using Approximations, Inst. Meas. Technol. Conf. (I2MTC), IEEE International, pp. 1923–1928, 2012.
25. J. L. Griggs, Albuquerque, NM, Private Communication, 14 December, 2011.
26. S. V. Patankar, *Numerical Heat Transfer and Fluid Flow*, Hemisphere Publishing Company, Washington, 1980.
27. H. K. Versteeg and W. Malalasekera, *An Introduction to Computational Fluid Dynamics: The Finite Volume Method*, Longman Group Ltd, Harlow, 1995.
28. J. H. Ferziger and M. Peric, *Computational Methods in Fluid Flow*, Springer-Verlag, New York, NY, 2002.